The Astrophysical Journal Letters, 879:L24 (5pp), 2019 July 10 https://doi.org/10.3847/2041-8213/ab2a72

A Hard Look at Thermal Reverberation and Optical/Ultraviolet Lags in NGC 5548

E. S. Kammoun[1], I. E. Papadakis[2,3,4], and M. Dovčiak[5]
[1] Department of Astronomy, University of Michigan, 1085 South University Avenue, Ann Arbor, MI 48109-1107, USA; ekammoun@umich.edu
[2] Department of Physics and Institute of Theoretical and Computational Physics, University of Crete, 71003 Heraklion, Greece
[3] Foundation for Research and Technology-Hellas, IESL, Voutes, 71110 Heraklion, Greece
[4] Institute of Astrophysics, FORTH, GR-71110 Heraklion, Greece
[5] Astronomical Institute of the Czech Academy of Sciences, Boční II 1401, CZ-14100 Prague, Czech Republic
Received 2019 May 7; revised 2019 June 17; accepted 2019 June 17; published 2019 July 10

Abstract

The ultraviolet (UV)/optical variations in many active galactic nuclei are very well correlated, showing delays that increase with increasing wavelength. It is thought that this is due to thermal reprocessing of the X-ray emission by the accretion disk. In this scenario, the variable X-ray flux from the corona illuminates the accretion disk where it is partially reflected, and partially absorbed and thermalized in the disk producing a UV/optical reverberation signal. This leads to time lags that increase with wavelength. However, although the shape of the observed time lags as a function of wavelength is consistent with the model predictions, their amplitude suggests the presence of a disk that is significantly hotter than expected. In this work, we estimate the response functions and the corresponding time lags assuming a standard Novikov–Thorne accretion disk illuminated by a point-like X-ray source. We take into account all relativistic effects in the light propagation from the X-ray source to the disk then to the observer. We also compute the disk reflection, accounting for its ionization profile. Our results show that thermal reverberation effects are stronger in sources with large X-ray source height and low accretion rate. We also found that the time lags increase with height and accretion rate. We apply our model to NGC 5548 and show that the observed lags in this source can be explained by the model for a source height of $\sim 60\ r_{\rm g}$ and an accretion rate of a few percent of the Eddington limit for a maximally spinning black hole.

Key words: galaxies: active – galaxies: individual (NGC 5548) – galaxies: Seyfert – X-rays: general

1. Introduction

Active galactic nuclei (AGNs) are thought to be powered by the accretion of matter onto a supermassive black hole (BH; with a mass $M_{\rm BH} \sim 10^{6-9}\ M_{\odot}$) in the form of an optically thick, geometrically thin disk (Novikov & Thorne 1973; Shakura & Sunyaev 1973). The disk emits a multi-temperature blackbody (BB) spectrum peaking in the ultraviolet (UV)/optical range. The temperature of the disk decreases with radius as $T(r) \propto r^{-3/4}$. A fraction of the disk photons are then Compton upscattered by a medium of hot electrons in the vicinity of the BH, the so-called "X-ray corona" (e.g., Shapiro et al. 1976; Haardt 1993). Several lines of evidence are suggestive of a compact corona located at a few gravitational radii ($r_{\rm g} = GM_{\rm BH}/c^2$) above the BH (e.g., Chartas et al. 2009; Fabian et al. 2009; De Marco et al. 2013; Reis & Miller 2013; Emmanoulopoulos et al. 2014).

In this case, X-rays from the corona irradiate the accretion disk. Some of them will be reprocessed and re-emitted in the form of the disk "X-ray reflection spectrum," while the rest will be absorbed and increase the disk's temperature. As a result, the UV/optical emission of the disk will be enhanced. Most of the UV photons are expected to emerge from the hot inner regions, while the optical photons are expected to be emitted by the cool outer regions. Consequently, if the X-rays are variable, we expect the disk UV/optical emission to also vary with a time lag that increases with wavelength.

Several multi-wavelength monitoring campaigns, using the *Neil Gehrels Swift Observatory* (*Swift*), have been performed recently to study AGN variability across X-rays, UV, and optical at high cadence and over long periods (e.g., McHardy et al. 2014, 2018; Shappee et al. 2014; Cackett et al. 2018; Edelson et al. 2019). In particular, Fausnaugh et al. (2016) studied the X-ray/UV/optical lags in NGC 5548 using data from the *Hubble Space Telescope (HST), Swift*, and ground-based telescopes. The authors showed that the measured lags are in agreement with the predicted $\tau \propto \lambda^{4/3}$ relation, in the case of a standard Shakura–Sunyaev disk. However, they also found that the time lags were larger than expected at all wavelengths.

In this Letter, we study the time lag versus wavelength relation (hereafter "lag-spectrum") in the context of the lamp-post geometry. We investigate the effects of the X-ray source height and the accretion rate on the reverberation signal and the lag spectra. Applying the model to NGC 5548, we find that a standard disk with a low accretion rate (~0.005–0.01 of the Eddington limit) is in agreement with the observed UV/optical lags in this source, as long as the X-ray source height is larger than 40 $r_{\rm g}$.

2. Model Setup

We consider a Keplerian, geometrically thin and optically thick accretion disk, around a BH of mass $M_{\rm BH}$ and accretion rate $\dot{m}$. The disk is co-rotating with the BH and its temperature profile follows the Novikov–Thorne prescription (Novikov & Thorne 1973), with a color temperature correction factor of 2.4. The disk extends from the innermost stable circular orbit (ISCO) at radius $r_{\rm ISCO}$, up to an outer radius of $r_{\rm out} = 10^4 r_{\rm g}$. The ISCO radius is uniquely defined by the BH spin. In this work, we consider two extreme cases, one with $a^* = 0$ ($r_{\rm ISCO} = 6\ r_{\rm g}$) and the other with $a^* = 1$ ($r_{\rm ISCO} = 1\ r_{\rm g}$). We also assume a point-like X-ray source located at a height (h) on the rotational axis of the BH (i.e., the lamp-post geometry). The X-rays are emitted isotropically (in the rest frame of the lamp-post) with an intrinsic spectrum

$F_X(t) = N(t)E^{-\Gamma}\exp(-E/E_C)$, and illuminates the disk. Part of this flux is reprocessed and re-emitted in X-rays (this is the "disk reflection component") and part of it is absorbed. We assume that the X-ray source is variable in normalization only.

Let us assume that the X-ray source emits a flash with flux F_{X0} at time t_0, with a duration Δt. Hence, an incident primary flux $F_{inc}(r, \tau')$ (in the disk's rest frame) will reach the disk at a radius r, and at a time τ'. If $F_{ref}(r, \tau')$ is the flux that is reflected from the disk, then

$$F_{abs}(r, \tau') = F_{inc}(r, \tau') - F_{ref}(r, \tau'), \quad (1)$$

is the flux absorbed by the disk. This flux is then added to the original disk flux assuming a Novikov–Thorne profile, $F_{NT}(r)$, and the sum can be used to estimate the disk temperature, as a function of radius and time, as follows:

$$T_{new}(r, \tau') = \left[\frac{F_{abs}(r, \tau') + F_{NT}(r)}{\sigma}\right]^{1/4}, \quad (2)$$

where σ is the Stefan–Boltzmann constant.

Then we compute the disk response, Ψ, to the short X-ray flash. To do that we identify all of the disk elements (in radius, r, and azimuth, φ) that a distant observer will "see" to be illuminated at the same time. Note that the temperature of each of these elements, T_{new}, will be different for each of them. Then we compute the flux that the observer receives, at a time τ_{obs}, from all of these elements in a given waveband, $\Delta\lambda$, between, say, λ_{min} and λ_{max}. Let us denote this flux as $F_{rev}(\Delta\lambda, \tau_{obs})$. Let us also denote with $F_{NT}(\Delta\lambda)$, the flux of these elements, in the same bandpass, when their temperature is equal to the Novikov–Thorne. We define the disk's "response function" in a given waveband as follows:

$$\Psi(\Delta\lambda, \tau_{obs}) = \frac{F_{rev}(\Delta\lambda, \tau_{obs}) - F_{NT}(\Delta\lambda)}{F_{X0}\,\Delta t}, \quad (3)$$

for each time, τ_{obs}, as the illumination progresses across the disk. The equation above shows the "extra" flux that is emitted by the disk, at each time τ_{obs} (in the observer's frame), due to the heating caused by the absorption of the incident X-rays. We note that the response function is normalized to the observed X-ray flux. The total (observed) flux emitted by the disk in the $\Delta\lambda$ band, and at time τ_{obs} will then be equal to

$$F_{obs}(\Delta\lambda, \tau_{obs}) = F_{NT}(\Delta\lambda) + \int_{-\infty}^{\infty} F_X(t')\Psi[\Delta\lambda, (\tau_{obs} - t')]dt'. \quad (4)$$

All the computations mentioned above were performed using the KYNXILREV[6] model (M. Dovčiak et al. 2019, in preparation). Given the *observed* 2–10 keV band luminosity of the X-ray source, the model estimates the intrinsic luminosity and the incident flux on each disk radius, as a function of time (in the observer's frame), taking into account all of the relativistic effects in the propagation of light from the primary source to the disk. Given the incident X-ray flux on the disk at each radius, the model estimates the radial ionization profile of the accretion disk assuming a constant disk density[7] (see Kammoun et al. 2019, for more details about the ionization estimates). The disk reflection spectrum is computed using the XILLVERD tables for the reflection spectrum from ionized material (García et al. 2016), by integrating them from 0.1 keV to infinity. The code then estimates $F_{abs}(r, \tau')$, $T_{new}(r, \tau')$, and, finally $\Psi(\lambda, \tau)$, taking into account all relativistic effects in the propagation of light from the X-ray source to the disk, and from the disk to the observer.

3. The Disk Response

To compute the disk response we chose model parameters values that are applicable for NGC 5548. In particular, we assumed an $M_{BH} = 5 \times 10^7\ M_\odot$(Bentz & Katz 2015), and an inclination of 40°. Using the results presented by Mathur et al. (2017), assuming a power-law photon index $\Gamma = 1.5$, we estimate the observed 2–10 keV luminosity of the source to be $L_X/L_{Edd} = 0.0034$. We also assumed a high-energy cutoff of 300 keV, and a luminosity distance of 75 Mpc as listed in the Simbad database (Wenger et al. 2000).

Using these values, we computed Ψ, considering eight values for the lamp-post height [h (r_g) = 2.5, 5, 10, 20, 40 ,60, 80, 100] and eight values of the accretion rate [$\dot{m}/\dot{m}_{Edd}(\%) = 0.25$, 0.5, 0.75, 1, 2.5, 5, 7.5, 10]. We assumed a disk density $n_H = 10^{17}$ cm^{-3}, and BH spins $a^* = 0$ and 1. We also consider the following wavebands presented by Fausnaugh et al. (2016): *HST* λ1158, *HST* λ1367, *HST* λ1746, *Swift* UVW2, *Swift* UVW1, and the *U, B, V, R, I* Johnson-Cousins. We assumed top-hat transmission curves for all filters, with a width of 5 Å for each of the *HST* bands, 1066 and 2892 Å for the *R* and *I* filters,[8] and the widths listed in Edelson et al. (2015) for the *UVW2, UVW1, U, B*, and *V* filters.

3.1. Effects of the Accretion Rate

The left panel of Figure 1 shows the response functions for all the values of $\dot{m}$, for $a^* = 0$ and 1, in the *HST* λ1158 and the *I* bands (the shortest and longest wavelengths, respectively), for $h = 10\ r_g$. First, the responses for all accretion rates and in both bands (actually in all bands) start rising at the same time. This is due to the fact that all disk elements emit a BB spectrum and, at the beginning, we observe elements close to the BH whose temperature is such that λ_{max} is shorter than 1158 Å. Consequently, the flux even at the shortest wavelengths will start increasing at the same time.

Second, Ψ increases in amplitude and gets narrower as the accretion rate decreases. The former effect is due to the fact that the disk temperature decreases with decreasing $\dot{m}$, thus $F_{NT}(r)$ is smaller. Consequently, for a constant X-ray luminosity, $F_{abs}(r)$ will increase, hence the disk excess flux (i.e., the disk response) will increase for lower $\dot{m}$ values. Regarding the second effect, we note that, in general, Ψ starts decreasing when the temperature of the disk elements, contributing to the observed flux in a given wavelength range, is so low such that the flux comes from the Wien part of the spectrum. As time passes, we observe emission from disk elements that are located farther out and are colder. As a result their emission at short wavelengths is diminished, hence the smaller width of response functions at short wavelengths (for all $\dot{m}$ and h, as seen in the next section). At the same time, as $\dot{m}$ decreases, the overall temperature (Equation (2)) decreases. Thus, the

[6] https://projects.asu.cas.cz/stronggravity/kynreverb/

[7] The choice of a constant disk density in the estimation of the ionization disk profile should not significantly affect our results because the radial dependence of any realistic density profile is much less significant than the radial decrease of the disk illumination by the lamp-post (see e.g., Svoboda et al. 2012; Kammoun et al. 2019).

[8] https://www.aip.de/en/research/facilities/stella/instruments/data/johnson-ubvri-filter-curves

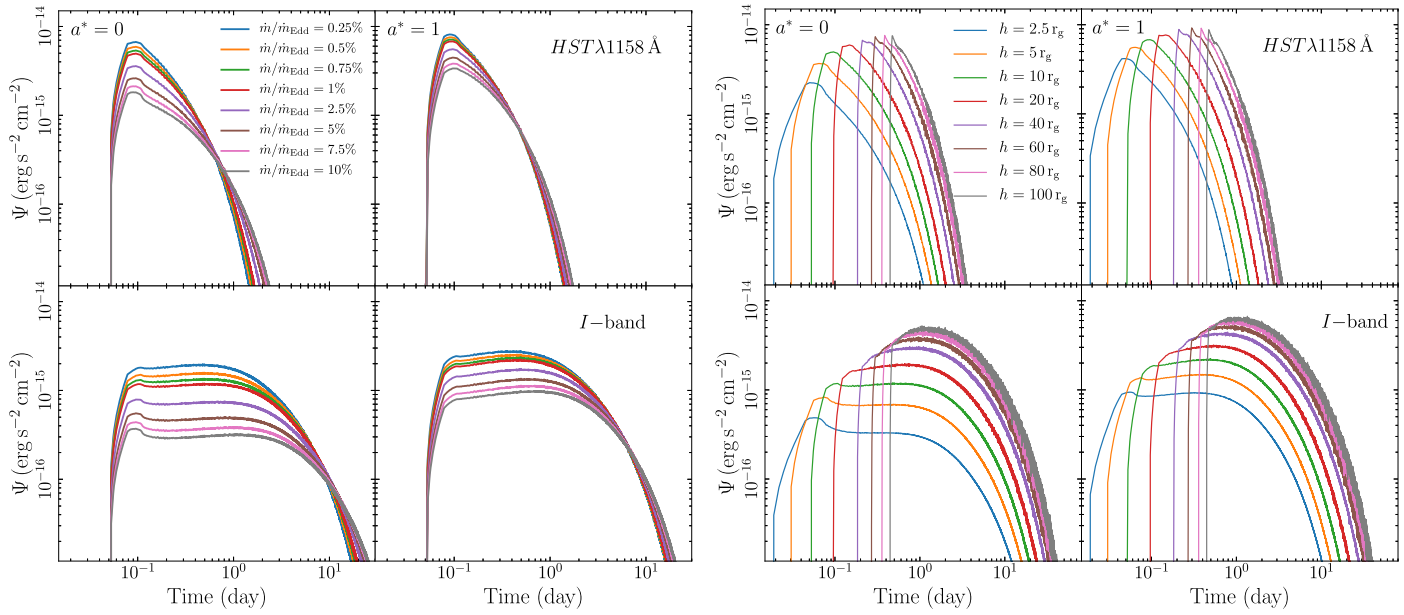

Figure 1. Left panel: response functions for the various $\dot{m}$ values we considered ($h = 10\,r_g$). Right panel: the same for the various h values that we considered ($\dot{m} = 0.01\,\dot{m}_{\rm Edd}$). Left and right columns correspond to $a^* = 0$ and 1, respectively. The top and bottom rows show the responses for the *HST* λ 1158 and the *I*-band, respectively.

response function (at a given wavelength) will start decreasing at earlier times, causing the full response function to be narrower for lower $\dot{m}$.

3.2. Effects of the Lamp-post Height

The right panel of Figure 1 shows the response functions for all the values of h, for spins 0 and 1, $\dot{m}/\dot{m}_{\rm Edd} = 1\%$, and the *HST* λ1158 and the *I* bands. As expected, the larger the height of the lamp-post, the later the response function starts and the longer it lasts. This is due to the light travel time from the X-ray source to the disk. In addition, the amplitude of the response functions increases with height. In fact, the incident flux is proportional to the cosine of the incident angle (defined as the angle between the normal to the disk plane and the photon trajectory; $\cos\theta_{\rm inc} = h/\sqrt{h^2 + r^2}$). Hence, by increasing the height $\cos\theta_{\rm inc}$ increases leading to a larger incident flux. This effect is mainly important for large radii, where the disk is completely neutral. At smaller radii, as the height increases, $\cos\theta_{\rm inc}$ still increases but the incident flux decreases due to the increase of the distance of the X-ray source to the disk. At the same time though, the ionization state of the inner parts of the disk decreases, which results in lower $F_{\rm ref}$, hence larger $F_{\rm abs}$. Combining both effects the amplitude of the response function increases with height.

We note that the response functions at low spin are broader and have lower amplitudes than the ones for $a^* = 1$. This is due to the fact that for the same $\dot{m}/\dot{m}_{\rm Edd}$ value, the physical value of $\dot{m}$ (in $M_\odot\,{\rm yr}^{-1}$) is higher in the low spin case.[9] Consequently, the disk is hotter and Ψ will have a lower amplitude and will be broader, as explained in the previous section.

[9] Because $\dot{m} = L/\eta c^2$, and the radiative efficiency η is smaller for a low spin, $\dot{m}$ (in physical units) is larger than for $a^* = 1$.

4. The Time Delays

Then, we estimate the centroid time delay of the transfer functions at a give wavelength (λ) as follows:

$$\langle\tau(\lambda)\rangle = \frac{\int \tau\Psi(\tau,\,\lambda)d\tau}{\int \Psi(\tau,\,\lambda)d\tau}. \quad (5)$$

It is this mean time lag that we can compare with the observed time lags between X-rays and UV/optical light curves. The left panels of Figure 2 show the dependence of $\langle\tau\rangle$ on $\dot{m}$ (for $a^* = 0$ and 1; $h = 10\,r_g$). The curves in the leftmost panel show that, at a given wavelength, the mean time lag increases with increasing $\dot{m}$. This is due to the fact that the width of the response increases with increasing $\dot{m}$. The mean time lag increases with the same rate in all wavebands. In addition, $\langle\tau\rangle$ is larger and increases in a steeper way with increasing $\dot{m}$ for a non-rotating BH compared to a maximally rotating one. This is due to the fact that the response width is larger and increases more with increasing $\dot{m}$ for $a^* = 0$ (see Figure 1).

The right panels of Figure 2 show the mean time lags as a function of source height ($\dot{m}/\dot{m}_{\rm Edd} = 1\%$). The mean time lag increases with the increase source height, as expected (as the respective responses are delayed and last longer as the height increases; see the right panels in Figure 1). The time lags at a given energy band are slightly larger in the $a^* = 0$ case, because the respective responses are wider.

5. The Case of NGC 5548

The filled points in Figure 3 represent the observed time lags between the X-ray and the UV/optical light curves in NGC 5548. They have been estimated by adding 0.65 day (i.e., the observed time lag between X-rays and the *HST*λ1367 light curve) to the time lags listed in Table 6 of Fausnaugh et al. (2016). We compared the observed time lags to our model predictions as follows.

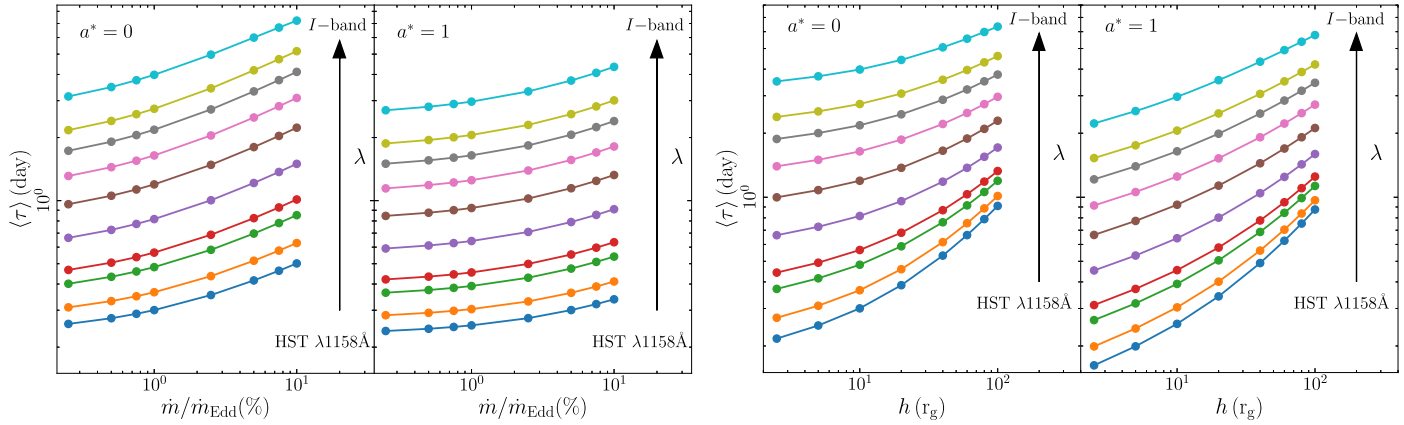

Figure 2. Left panel: mean time delay as function of $\dot{m}(h = 10\ r_{\rm g})$. Right panel: mean time delay as function of h ($\dot{m}/\dot{m}_{\rm Edd} = 1$ %). The left and right plots in each panel correspond to $a^* = 0$ and 1, respectively. Time delays are shown for all wavebands, increasing λ from bottom to top.

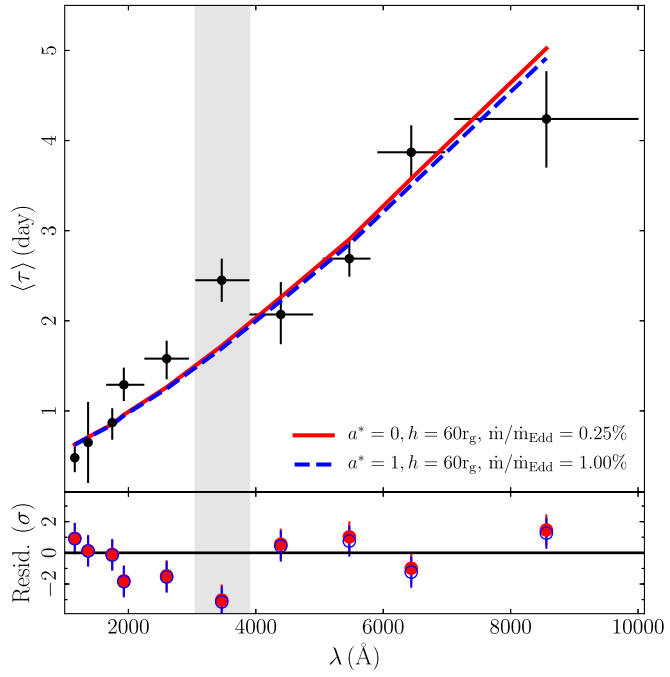

Figure 3. Best-fit models for $a^* = 0$ (solid line) and $a^* = 1$ (dashed line) obtained by fitting the observed time lags, excluding the measurement in the U-band (shaded region; see Section 5 for details).

We estimated the χ^2 between the model lag-spectra (for all $\dot{m}$ and heights; 64 in total for each spin) and the data, and we chose the model time lags with the minimum χ^2 value ($\chi^2_{\rm min}$). The fit was not statistically acceptable either for $a^* = 0$ or for $a^* = 1$, $\chi^2_{\rm min} = 19.9/8$ degrees of freedom (dof), and $19.2/8$, respectively. This is most likely due to the fact that the time lag in the U-band appears to be larger compared to the general trend. This was already noticed by Edelson et al. (2015) and Fausnaugh et al. (2016), and is probably due to an additional delay caused by the Balmer jump (Korista & Goad 2001). We re-fitted the observed lags by excluding the U-band point from the fit. In this case, we obtained statistically accepted fits with $\chi^2_{\rm min}/{\rm dof} = 10.8/7$ and $10.7/7$ (p-value $= 0.15$ and 0.16) for $a^* = 0$ and $a^* = 1$, respectively. The solid (dashed) lines in the same figure indicate the best-fit model to the observed lag spectrum for $a^* = 0$ ($a^* = 1$). We note that some deficit can be seen in the I-band, though not statistically significant. This might be due to $r_{\rm out}$ being smaller than $10^4\ r_{\rm g}$.

The best-fit values of height and accretion rate are ($60\ r_{\rm g}$, 0.25%) and ($60\ r_{\rm g}$, 1%) for $a^* = 0$ and $a^* = 1$, respectively. The best-fit $\dot{m}$ in the case of a non-rotating BH coincides with the lowest value that we considered, with a 3σ upper limit of 2.5%. The 1σ confidence region of $\dot{m}$ for $a^* = 1$ is 0.25%–2.5%. The best-fit accretion rates correspond to 0.0048 and 0.0026 $M_\odot\ {\rm yr}^{-1}$ for $a^* = 0$ and $a^* = 1$, respectively. Their difference is smaller than the difference of the best-fit values in Eddington units. The best-fit heights are identical in both cases, with the 3σ confidence region being (40–80 $r_{\rm g}$) and (20–80 $r_{\rm g}$) for $a^* = 0$ and $a^* = 1$, respectively.

6. Conclusions

We calculate the disk response functions in various wavebands when it is illuminated by X-rays assuming a lamp-post geometry. We consider all relativistic effects in the light propagation from the X-ray source to the disk and from the disk to the observer. We also account for the disk X-ray reflection by computing the disk ionization at each radius. We found that: (i) the delays between X-rays and optical/UV bands increase with increasing source height and increasing accretion rate, and (ii) the disk response in all UV/optical bands increases when the source height increases and the accretion rate decreases. Therefore, we do not expect a strong thermal reverberation signal in objects with high accretion rate and strong X-ray reflection signatures like, for example, the X-ray bright narrow-line Seyfert-1 galaxies.

Using reasonable values for the model parameters (i.e., BH mass, inclination, X-ray spectral slope, and mean flux) we explained that the observed time-lag spectrum in NGC 5548. The best-fit results indicate a source height larger than 20 or 40 $r_{\rm g}$ (3σ limit for $a^* = 1$ or 0, respectively). This is significantly larger than 4–5 $r_{\rm g}$, which is the height estimate from the modeling of the X-ray time lags in a few bright Seyferts, assuming the same geometry (i.e., Emmanoulopoulos et al. 2014; Chainakun et al. 2016; Epitropakis et al. 2016; Caballero-García et al. 2018). Nevertheless, our results are in agreement with Brenneman et al. (2012), who inferred a height of the X-ray source in NGC 5548 $\sim$100 $r_{\rm g}$. An alternative solution is provided by Gardner & Done (2017). Their model consists of a puffed-up, Comptonized inner disk region. They proposed that that the continuum UV/optical lags are due to the expansion/contraction of this region, in both radius and height, in response to the variable X-ray heating of its inner

edge. We also note that our results depend on the assumption of a thin, plane-parallel Novikov–Thorne disk. Different disk geometries (for example, a tilted disk; Nealon et al. 2015) might affect the source height estimation; however, exploring this goes beyond the scope of our work.

As for the accretion rate, the best-fit values indicate rates which are ∼1% of the Eddington limit. According to Fausnaugh et al. (2016), the mean source flux at 5100 Å is $\sim 4.6 \times 10^{-11}$ erg s^{-1} cm^{-2}. Assuming a bolometric correction factor of 7.8 ± 1.7 (Krawczyk et al. 2013), this implies a bolometric luminosity of $(2.5 \pm 0.5) \times 10^{44}$ erg s^{-1}, which is 0.034 ± 0.008 of the Eddington luminosity limit for $M_{\rm BH} = 5.7 \times 10^7\ M_{\odot}$. This value is at odds with the $\dot{m}$ estimate for $a^* = 0$ (the 3σ upper limit is just 0.025), but is entirely consistent with the $\dot{m}$ estimate considering a standard accretion disk around a maximally rotating BH.

Contrary to our results, Starkey et al. (2017) found that a standard disk, with a low $\dot{m}$, is ruled out by the data. A significant difference between their and our modeling is that they kept h fixed at 6 $r_{\rm g}$ and let the inclination free, while we fixed the inclination to 40° and let h free. In addition, we do not assume a fixed albedo for the disk, but we compute the flux that is reflected by the disk, at each radius, based on its ionization state accounting for all relativistic effects. Furthermore, we compute the time lags using the model disk response functions, without assuming that all variations in the UV/optical light curves are due to thermal reverberation. In the future, we plan to compare the model with the observed UV/optical light curves, as this will be a crucial test for the model.

M.D. thanks MEYS of Czech Republic for the support through the 18-00533S research project and his home institution, ASU, supported by the project RVO:67985815. I. P. would like to thank ASU for their hospitality.

ORCID iDs

E. S. Kammoun https://orcid.org/0000-0002-0273-218X
M. Dovčiak https://orcid.org/0000-0003-0079-1239

References

Bentz, M. C., & Katz, S. 2015, PASP, 127, 67
Brenneman, L. W., Elvis, M., Krongold, Y., Liu, Y., & Mathur, S. 2012, ApJ, 744, 13
Caballero-García, M. D., Papadakis, I. E., Dovčiak, M., et al. 2018, MNRAS, 480, 2650
Cackett, E. M., Chiang, C.-Y., McHardy, I., et al. 2018, ApJ, 857, 53
Chainakun, P., Young, A. J., & Kara, E. 2016, MNRAS, 460, 3076
Chartas, G., Kochanek, C. S., Dai, X., Poindexter, S., & Garmire, G. 2009, ApJ, 693, 174
De Marco, B., Ponti, G., Cappi, M., et al. 2013, MNRAS, 431, 2441
Edelson, R., Gelbord, J., Cackett, E., et al. 2019, ApJ, 870, 123
Edelson, R., Gelbord, J. M., Horne, K., et al. 2015, ApJ, 806, 129
Emmanoulopoulos, D., Papadakis, I. E., Dovčiak, M., & McHardy, I. M. 2014, MNRAS, 439, 22
Epitropakis, A., Papadakis, I. E., Dovčiak, M., et al. 2016, A&A, 594, A71
Fabian, A. C., Zoghbi, A., Ross, R. R., et al. 2009, Natur, 459, 540
Fausnaugh, M. M., Denney, K. D., Barth, A. J., et al. 2016, ApJ, 821, 56
García, J. A., Fabian, A. C., Kallman, T. R., et al. 2016, MNRAS, 462, 751
Gardner, E., & Done, C. 2017, MNRAS, 470, 3591
Haardt, F. 1993, ApJ, 413, 680
Kammoun, E. S., Domček, V., Svoboda, J., Dovčiak, M., & Matt, G. 2019, MNRAS, 485, 239
Korista, K. T., & Goad, M. R. 2001, ApJ, 553, 695
Krawczyk, C. M., Richards, G. T., Mehta, S. S., et al. 2013, ApJS, 206, 4
Mathur, S., Gupta, A., Page, K., et al. 2017, ApJ, 846, 55
McHardy, I. M., Cameron, D. T., Dwelly, T., et al. 2014, MNRAS, 444, 1469
McHardy, I. M., Connolly, S. D., Horne, K., et al. 2018, MNRAS, 480, 2881
Nealon, R., Price, D. J., & Nixon, C. J. 2015, MNRAS, 448, 1526
Novikov, I. D., & Thorne, K. S. 1973, in Black Holes (Les Astres Occlus), ed. C. Dewitt & B. S. Dewitt (New York: Gordon and Breach), 343
Reis, R. C., & Miller, J. M. 2013, ApJL, 769, L7
Shakura, N. I., & Sunyaev, R. A. 1973, A&A, 24, 337
Shapiro, S. L., Lightman, A. P., & Eardley, D. M. 1976, ApJ, 204, 187
Shappee, B. J., Prieto, J. L., Grupe, D., et al. 2014, ApJ, 788, 48
Starkey, D., Horne, K., Fausnaugh, M. M., et al. 2017, ApJ, 835, 65
Svoboda, J., Dovčiak, M., Goosmann, R. W., et al. 2012, A&A, 545, A106
Wenger, M., Ochsenbein, F., Egret, D., et al. 2000, A&AS, 143, 9